MIT
Center for Space Research   Chandra X-Ray Center

MEMORANDUM
May 3, 2004

To:	Dale Graessle, CALDB lead
From:	Bish K. Ishibashi, SDS
Subject:	Evaluation on the quality of HETG/ACIS-S LSFPARM file for unrandomized event datasets
Revision:	1.1
URL:	http://space.mit.edu/CXC/docs/memo_lsf_ha_1.1.ps
File:	/nfs/cxc/h2/bish/CXC SDS/LSFDIR/HO_LSF_HA/memo_lsf_ha_1.1.tex

1 Unrandomized LSFPARM files for HETG/ACIS-S Configuration

In Repro *III*, decisions have been made to turn off data randomization on TG R/D. This action necessitates rapid development of line spread function parameter files (LSFPARM) without built-in data randomization. By applying the similar LSF processing scheme[1], new LSFPARM files for HETG+ACIS-S configuration have been developed. This document describes the quality of the new LSFPARM products.

2 Building LSFPARM

Procedures for building a LSFPARM file is described at:

http://space.mit.edu/CXC/LSFX/LSF_valid2.html

For rapid development, several parts of IDL parameterization routines are S-Langified for better and faster convergence to optimum fitting parameters through automated processes.

3 Data products

Four LSFPARM products are developed: HEG and MEG $\pm$ 1^{st} orders configuration with HETG+ACIS-S without data randomization in TG coordinate. Evaluation of the four products are documented in the following section.

[1]See an example in https://icxc.harvard.edu/calco/ard_updates/ECR/Approved_ECRs/ECR_2002_016.html

Table 1. New header keywords for LSFPARM

Keyword	Value	Comment
RAND_TG	0.0	No data randomization in TG values
CBD60001	RAND_TG(0.0)	CALDB query expression

3.1 Header Keyword for Data Randomization

Two new FITS header keywords – RAND_TG and CBD60001 – are included in each LSFPARM product in order to specify whether LSFPARM products is for randomized or not. For unrandomized dataset, these header keywords are set to the values as listed in Table 1. These keywords would enable to form proper CALDB query expression and to search for unrandomized LSFPARM products.

4 Testing LSFPARM products

4.1 Procedures

Testing of the LSFPARM products are performed with MARX simulated and real Capella (ObsID 1103) datasets. Two key points of our interests are (1) line profile and (2) encircled energy fractions (hereafter EEFRAC).

4.2 Evaluation I. MARX-Simulated Dataset

Mono-energetic beam simulations are performed with MARX at various energy values and concatenated together to make a L1 event file. The L1 file has gone through nominal CIAO processing, except that pixel randomization in TG space being turned off at *tg_resolve_events*. Corresponding grating RMF files are generated via *mkgrmf* command with the new LSFPARM files and used as a fitting kernel in *ISIS* for evaluation. Cash statistics is applied throughout this work.

4.2.1 Line Profile Analysis

If the LSFPARM products are valid, simulated line profiles can be described with a Kronecker delta function folded over grating RMFs. Figures 1 through 4 show several line profiles fitted with a delta function. For brevity, selected four of 21 line samples are shown in each figure for inspection: lines at E = 800, 1400, 1800, and 6500 eV. These are representative of the results of other line profile fittings, resulting in the value of goodness of fit generally less than 1.1 for HEG and 1.5 for MEG (these are not meant to be necessarily the best fitting results).

Despite unusually high S/N ratio in these line profile simulations, the model fitting has resulted in the low χ^2 values and hence the results validate that the LSF parameterization (used earlier in recent LSF works) works here just as well as before.

4.2.2 Encircled Energy Fraction

The second key component of LSFPARM products is the value of encircled energy fraction as a function of energy. The value EEFRAC is derived from cross-dispersion line profile of a mono-energetic beam, integrated over arbitrary extraction width centered around the line peak (or in Chandra's term, at TG_D = 0 degree). If derived correctly, EEFRAC will allow users to correct measured count rates (or fluxes) for the aperture of the extraction.

The following tests are performed such that the simulated line spectra (samples shown in Figures 1 – 4) are extracted at five different aperture widths; then the delta-function model is fitted to 22 mono-energetic lines in order to derive model line fluxes F_m in counts s^{-1}. ISIS is also enabled to provide cumulative counts in each line, which is used to derive a "observed" line flux F_d. In an ideal condition, both the model and observed line fluxes should be identical, i.e.,

$$\frac{F_d}{F_m} \approx 1.$$

All four configurations (HEG and MEG $\pm$ 1st) are tested and verified that the new LSFPARM products meet this criterion within a few percentage (see Tables 2 – 5), presumably better than our knowledge in effective area of Chandra's HRMA system.

Note that the ratio value is consistently equal to or slightly higher than 1 for all configurations.

4.3 Evaluation II. Chandra Dataset

The same four LSFPARM products are tested against real Chandra observation (Capella, ObsID = 1103) in the similar manner as performed on the simulated datasets.

4.3.1 Line Profile Analysis

Instead of using a delta function, thermal X-ray APED model and simple Gaussian function are fitted on the emission spectrum of Capella. Five to eight bright emission lines – Si XIII, Mg XI and Mg XII, Ne X, Fe XVII, O VII and O VIII, and N VII – are selected for testing. Upon fitting the parameter for line width dv (converted to velocity scale in km s^{-1}) is allowed to vary. Ideally the parameter dv should be ≈ 0 km s^{-1} for thermal APED modeling; however, for Gaussian fitting, the value dv is expected to be ≥ 0 km s^{-1} as most of these lines are either H-like doublet lines or blended with other weak atomic lines. The results of fitting with the APED model is tabulated in Tables 6 – 9; likewise, the results with the Gaussian model in Tables 10 – 13. Corresponding figures for line profile fit are shown in Figures 5 – 8 for the APED model and in Figures 9 – 12 for the Gaussian model . These are, once again, not meant to be the best fitting parameters.

Upon inspection of Tables 6 – 9, it is noted that the measured line width is consistent with 0 km s^{-1} for the most of lines. A notable exception is a strong Fe XVII line λ 15.014, which consistently shows positive measured widths in all HETG configurations. It is not clear if this is a failure in the LSFPARM products or is it a detection of small line broadening in Capella's system. Moreover, it is possible that the model is not adequate for this line.

The same practice with the Gaussian model is repeated and their results show some positive measured line widths, just as expected from blended lines. The positive line widths are more notable with HEG configuration, implying that some doublet lines – separated by 0.0050Å– are marginally resolved. To verify this point, I have explored the parameter space in Gaussian width and wavelength to see how significant the detection of non-zero line width is. Figure 13 illustrates that all H-like doublet lines have the measurable widths of $\approx$ 0.003 – 0.004Å.

All of the line plots (Figures 5 – 12) show a reasonably good fit to their spectral line profiles. Some lines are more susceptible to line blends which are not carefully dealt with in these exercise.

4.3.2 Encircled Energy Fraction

Lastly the model EEFRAC values need to be compared with the observed ones. Here we first compute the theoretical EEFRAC values at three different aperture widths based on the new LSFPARM products. Then at the same aperture widths extract spectra from observed event datasets. Two targets are chosen for this exercise: Capella[2] and X-ray binary X1543-62. Since absolute spectral energy distributions of these targets are not known, the ratio of two entities are compared instead. Here in this exercise, the ratio of the observed spectra "Extraction B" (at a width equivalent to EEFRAC = 80% at E = 1.497keV) to "Extraction A" (similarly at EEFRAC = 98.5%, or nearly at CIAO default extraction width) is compared with the theoretical counterpart. The same exercise is repeated for "Extraction C" (at EEFRAC = 60%) as well.

[2]All the Capella datasets are combined for this purpose.

If the EEFRAC values in the LSFPARM products are derived properly, the ratio (as a function of wavelength) should be consistent to each other. Figure 14 shows the ratio plots for every HETG configuration derived with the Capella dataset. Figure 15 shows the same for X1543-62. As shown in these figures, the model trend agrees well within a few percentages with the observed trend for all cases. Small deviation between the theoretical and observed ratios is noted in the MEG configuration for X1543-62, although the difference is only about 5%; and a number of possible sources for uncertainties may explain such difference.

5 Summary

All the testings show that the quality of these new LSFPARM products for unrandomized datasets are equally as good as the earlier LSFPARM products produced through the same LSF generation scheme. While some anomalous (but minute) differences are found in both line profile and EEFRAC analyses, the difference may originate due to some unidentified calibration issues not included in the current MARX distribution.

Table 2. HEG +1st: the Data-to-Model flux ratio

Energy (keV)	Widths (radian)				
	2.84e-4	4.19e-4	5.35e-4	7.09e-1	1.41e-3
0.8	1.11	1.10	1.02	1.01	1.00
1.0	1.00	1.03	1.00	1.04	1.02
1.2	1.00	1.01	1.01	1.02	1.02
1.4	1.01	1.01	1.01	1.01	1.01
1.6	1.02	1.01	1.01	1.01	1.01
1.8	1.02	1.02	1.02	1.02	1.02
2.0	1.01	1.01	1.01	1.01	1.01
2.2	1.02	1.02	1.01	1.01	1.01
2.4	1.03	1.03	1.03	1.02	1.02
2.6	1.03	1.02	1.03	1.03	1.03
2.8	1.03	1.02	1.02	1.01	1.02
3.0	1.01	1.02	1.02	1.00	1.01
3.2	1.02	1.01	1.01	1.01	1.02
3.4	1.02	1.02	1.02	1.02	1.02
3.6	1.02	1.01	1.01	1.01	1.01
3.8	1.01	1.01	1.01	1.01	1.01
4.0	1.03	1.02	1.02	1.02	1.02
4.5	1.02	1.01	1.01	1.01	1.01
5.0	1.02	1.02	1.02	1.02	1.02
6.0	1.02	1.02	1.03	1.02	1.03
6.5	1.00	1.02	1.00	1.00	1.00

Table 3. HEG -1st: the Data-to-Model flux ratio

Energy (keV)	Widths (radian)				
	2.84e-4	4.19e-4	5.35e-4	7.09e-1	1.41e-3
0.8	1.00	1.03	1.03	1.03	1.03
1.0	1.01	1.01	1.01	1.01	1.01
1.2	1.01	1.01	1.01	1.01	1.01
1.4	1.02	1.02	1.01	1.01	1.01
1.6	1.01	1.01	1.01	1.01	1.01
1.8	1.01	1.01	1.01	1.01	1.01
2.0	1.01	1.01	1.01	1.01	1.01
2.2	1.02	1.02	1.02	1.02	1.02
2.4	1.03	1.03	1.03	1.03	1.03
2.6	1.03	1.02	1.02	1.02	1.02
2.8	1.02	1.02	1.02	1.02	1.02
3.0	1.02	1.02	1.02	1.02	1.02
3.2	1.01	1.01	1.01	1.01	1.02
3.4	1.02	1.02	1.02	1.02	1.02
3.6	1.02	1.02	1.02	1.03	1.02
3.8	1.02	1.02	1.02	1.02	1.02
4.0	1.02	1.02	1.02	1.02	1.02
4.5	1.03	1.02	1.02	1.02	1.02
5.0	1.02	1.01	1.01	1.01	1.04
6.0	1.00	1.01	1.01	1.01	1.01
6.5	1.00	1.01	1.00	1.01	1.00

Table 4. MEG +1st: the Data-to-Model flux ratio

Energy (keV)	Widths (radian)				
	2.84e-4	4.19e-4	5.35e-4	7.09e-1	1.41e-3
0.8	1.11	1.08	1.05	1.05	1.03
1.0	1.01	1.01	1.01	1.01	1.00
1.2	1.03	1.02	1.02	1.02	1.02
1.4	1.02	1.02	1.02	1.02	1.02
1.6	1.02	1.01	1.01	1.01	1.01
1.8	1.02	1.02	1.02	1.02	1.02
2.0	1.01	1.01	1.01	1.01	1.01
2.2	1.02	1.02	1.02	1.02	1.02
2.4	1.04	1.03	1.03	1.03	1.03
2.6	1.04	1.04	1.03	1.03	1.03
2.8	1.02	1.02	1.01	1.01	1.01
3.0	1.02	1.02	1.01	1.01	1.01
3.2	1.03	1.02	1.02	1.02	1.02
3.4	1.01	1.01	1.01	1.01	1.01
3.6	1.02	1.01	1.02	1.02	1.02
3.8	1.02	1.02	1.02	1.01	1.01
4.0	1.02	1.02	1.02	1.02	1.02
4.5	1.02	1.02	1.02	1.02	1.02
5.0	1.01	1.01	1.01	1.01	1.01
6.0	1.03	1.02	1.02	1.02	1.02
6.5	1.03	1.03	1.03	1.03	1.03

Table 5. MEG -1st: the Data-to-Model flux ratio

Energy (keV)	Widths (radian)				
	2.84e-4	4.19e-4	5.35e-4	7.09e-1	1.41e-3
0.8	1.01	1.02	1.01	1.01	1.02
1.0	1.02	1.01	1.01	1.01	1.01
1.2	1.01	1.01	1.01	1.01	1.01
1.4	1.01	1.01	1.01	1.01	1.01
1.6	1.01	1.01	1.01	1.01	1.01
1.8	1.01	1.01	1.01	1.01	1.01
2.0	1.02	1.02	1.01	1.02	1.01
2.2	1.03	1.02	1.02	1.02	1.02
2.4	1.03	1.03	1.02	1.02	1.02
2.6	1.03	1.03	1.03	1.03	1.03
2.8	1.02	1.02	1.03	1.03	1.02
3.0	1.03	1.03	1.03	1.03	1.02
3.2	1.03	1.02	1.02	1.02	1.02
3.4	1.02	1.02	1.02	1.02	1.02
3.6	1.02	1.01	1.01	1.02	1.01
3.8	1.03	1.03	1.03	1.03	1.03
4.0	1.02	1.02	1.02	1.02	1.02
4.5	1.04	1.03	1.03	1.03	1.03
5.0	1.03	1.03	1.02	1.03	1.02
6.0	1.09	1.09	1.08	1.08	1.07
6.5	1.10	1.04	1.04	1.04	1.04

Table 6. Capella HEG +1st: thermal APED model.

Element	λ_{lab} (Å)	dv (km/s)	dv 3σ range	χ^2	Comment
Si XIII	6.6479	0.56	0 – 124	1.70	He-like triplet lines
Mg XII	8.4192	0.29	0 – 125	1.69	H-like doublet lines
Mg XI	9.1687	0.06	0 – 75.9	1.54	He-like triplet lines
Ne X	12.1321	0.01	0 – 128	1.52	Ne X and Fe XVII blend
Fe XVII	15.0140	54.7	20.8 – 119	2.04	Expected thermal width $\approx$ 38km/s

Table 7. Capella HEG -1st: thermal APED model.

Element	λ_{lab} (Å)	dv (km/s)	dv 3σ range	χ^2	Comment
Si XIII	6.6479	1.03	0 – 149	1.72	He-like triplet lines
Mg XII	8.4192	0.31	0 – 143	1.23	H-like doublet lines
Mg XI	9.1687	78.0	0 – 127	2.02	He-like triplet lines
Ne X	12.1321	95.7	31.2 – 172	1.16	Ne X and Fe XVII blend
Fe XVII	15.0140	76.0	52.9 – 122	2.02	Expected thermal width $\approx$ 38km/s

Table 8. Capella MEG +1st: thermal APED model.

Element	λ_{lab} (Å)	dv (km/s)	dv 3σ range	χ^2	Comment
Si XIII	6.6479	17.2	0 – 151	3.37	He-like triplet lines
Mg XII	8.4192	3.03	0 – 124	1.24	H-like doublet lines
Mg XI	9.1687	0.0	0 – 92.0	3.28	He-like triplet lines
Ne X	12.1321	0.08	0 – 67.7	2.23	Ne X and Fe XVII blend
Fe XVII	15.0140	54.8	0 – 121	4.48	Poor modeling on the neighboring lines
O VIII	18.9671	1.40	0 – 90.3	1.86	H-like doublet lines
O VII	21.6015	10.0	0 – 206	0.801	Weak line
N VII	24.7792	5.85	0 – 212	0.953	Weak line

Table 9. Capella MEG -1st: thermal APED model.

Element	λ_{lab} (Å)	dv (km/s)	dv 3σ range	χ^2	Comment
Si XIII	6.6479	0.01	0 – 120	2.45	He-like triplet lines
Mg XII	8.4192	0.0	0 – 184	1.26	H-like doublet lines
Mg XI	9.1687	0.0	0 – 47.4	2.59	He-like triplet lines
Ne X	12.1321	0.0	0 – 139	2.23	Ne X and Fe XVII blend
Fe XVII	15.0140	93.8	71.5 – 131	8.64	Poor modeling on the neighboring lines
O VIII	18.9671	50.5	0 – 110	2.38	H-like doublet lines
O VII	21.6015	72.1	0 – 141	1.34	Weak line
N VII	24.7792	2.56	0 – 116	1.42	Weak line

Table 10. Capella HEG +1st: Simple Gaussian model.

Element	λ_{lab} (Å)	dv (km/s)	dv 3σ range	χ^2	Comment
Si XIII	6.6479	87.6	0 – 196	2.94	blend
Mg XII	8.4192	83.2	40.9 – 165	1.81	doublet lines blended
Mg XI	9.1687	41.7	0 – 103	1.26	He-like triplet lines
Ne X	12.1321	151	127 – 181	1.80	Strong Ne X and Fe XVII blend
Fe XVII	15.0140	47.8	13.8 – 76.7	1.92	Expected thermal width $\approx$ 38km/s

Table 11. Capella HEG -1st: Simple Gaussian model.

Element	λ_{lab} (Å)	dv (km/s)	dv 3σ range	χ^2	Comment
Si XIII	6.6479	110	78.7 – 110	0.677	blend
Mg XII	8.4192	106	64.4 – 158	1.32	doublet lines blended
Mg XI	9.1687	104	77.7 – 162	2.25	He-like triplet lines
Ne X	12.1321	161	141 – 202	1.58	Strong Ne X and Fe XVII blend
Fe XVII	15.0140	47.1	16.6 – 75.0	1.88	Expected thermal width $\approx$ 38km/s

Table 12. Capella MEG +1st: Simple Gaussian model.

Element	λ_{lab} (Å)	dv (km/s)	dv 3σ range	χ^2	Comment
Si XIII	6.6479	0.0	0 – 0.01	2.26	He-like triplet lines
Mg XII	8.4192	30.0	0 – 107	1.09	H-like doublet lines
Mg XI	9.1687	19.0	0 – 93.6	0.972	He-like triplet lines
Ne X	12.1321	123	83.5 – 157	2.21	Ne X and Fe XVII blend
Fe XVII	15.0140	29.2	1.12 – 58.9	2.29	Poor modeling on the neighboring lines
O VIII	18.9671	47.8	0.285 – 96.1	1.67	H-like doublet lines
O VII	21.6015	5.42	0 – 192	1.26	Weak line
N VII	24.7792	35.8	0 – 144	0.926	Weak line

Table 13. Capella MEG -1st: Simple Gaussian model.

Element	λ_{lab} (Å)	dv (km/s)	dv 3σ range	χ^2	Comment
Si XIII	6.6479	0.92	0 – 134	1.40	He-like triplet lines
Mg XII	8.4192	119	0 – 196	1.47	H-like doublet lines
Mg XI	9.1687	24.9	0 – 75.0	1.07	He-like triplet lines
Ne X	12.1321	148	116 – 173	1.53	Ne X and Fe XVII blend
Fe XVII	15.0140	20.1	0.09 – 56.6	3.75	Poor modeling on the neighboring lines
O VIII	18.9671	77.8	61.4 – 111	2.06	H-like doublet lines
O VII	21.6015	0.20	0 – 91.8	4.03	Weak line
N VII	24.7792	0.108	0 – 80.4	1.35	Weak line

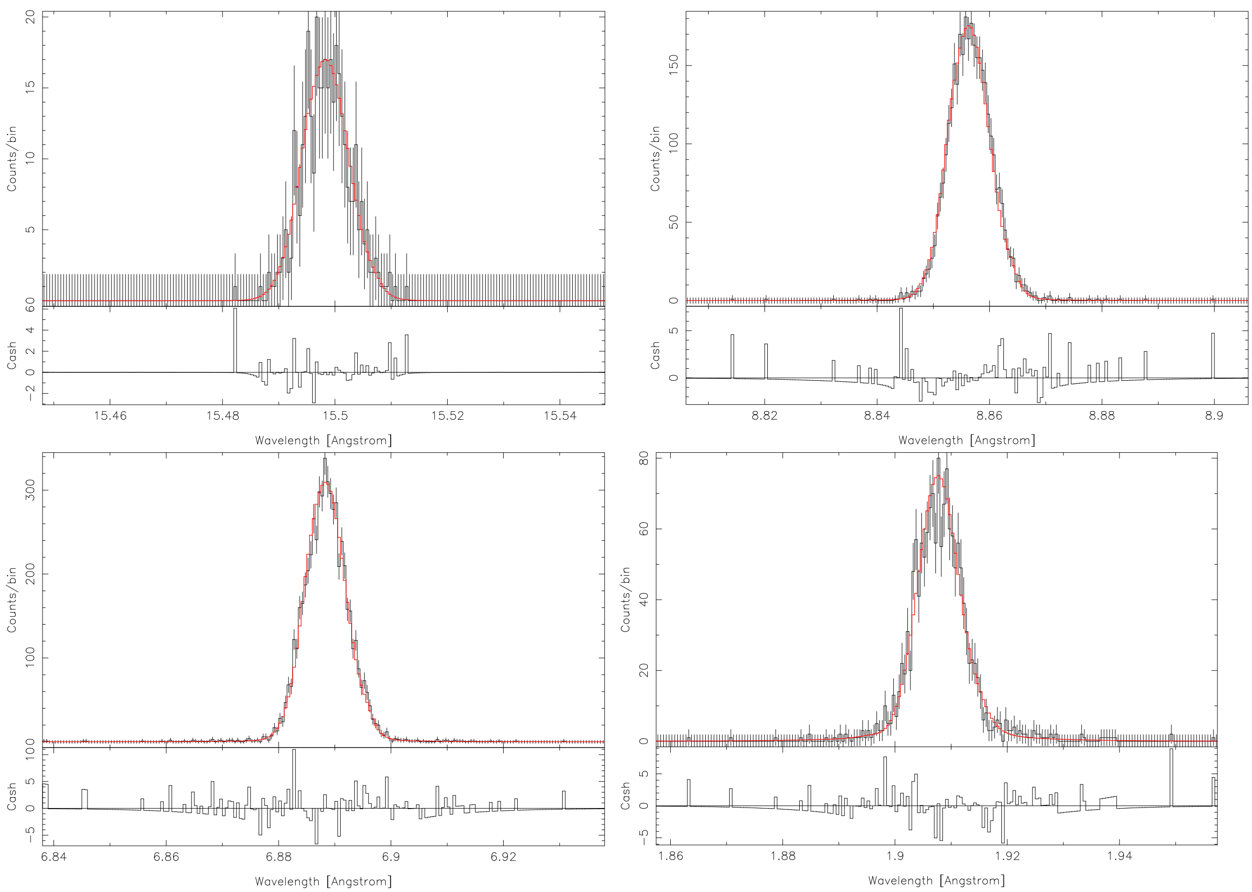

Figure 1: HEG +1st-order line profiles, fitted with a Kronecker delta function (red) folded over HEG +1st order grating RMF: (top left) line profile at E = 800 eV, with a goodness of fit χ^2 = 0.23; (top right) E = 1400 eV, χ^2 = 0.63; (bottom left) E = 1800 eV, χ^2 =1.0; and (bottom right) E = 6500 eV, χ^2 = 0.88. The delta function model describes simulated line profiles fairly well, which validates my scheme for LSF parameterization.

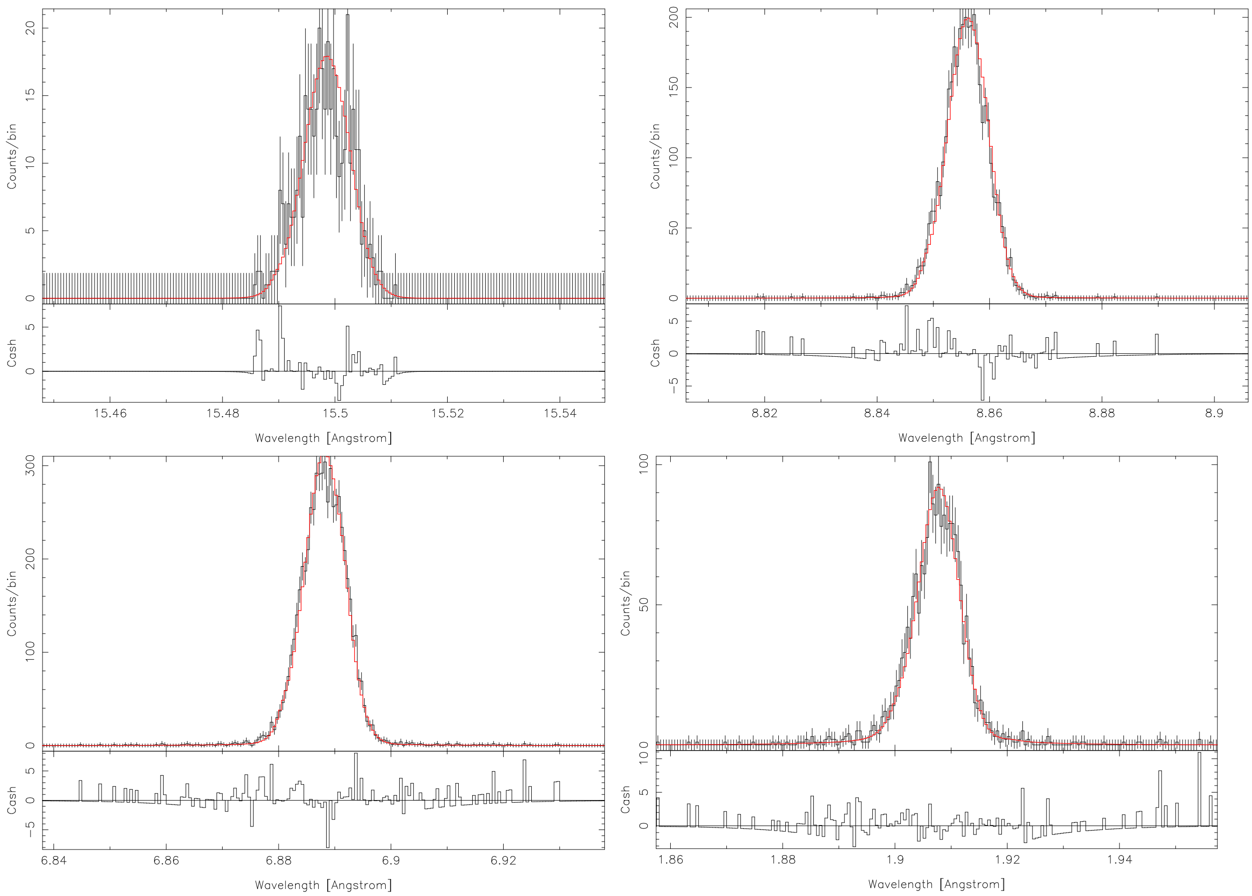

Figure 2: HEG -1st-order line profiles: (top left) line profile at E = 800 eV, with a goodness of fit $\chi^2 = 0.30$; (top right) E = 1400 eV, $\chi^2 = 0.67$; (bottom left) E = 1800 eV,χ^2 =1.0; and (bottom right) E = 6500 eV, $\chi^2 = 1.0$.

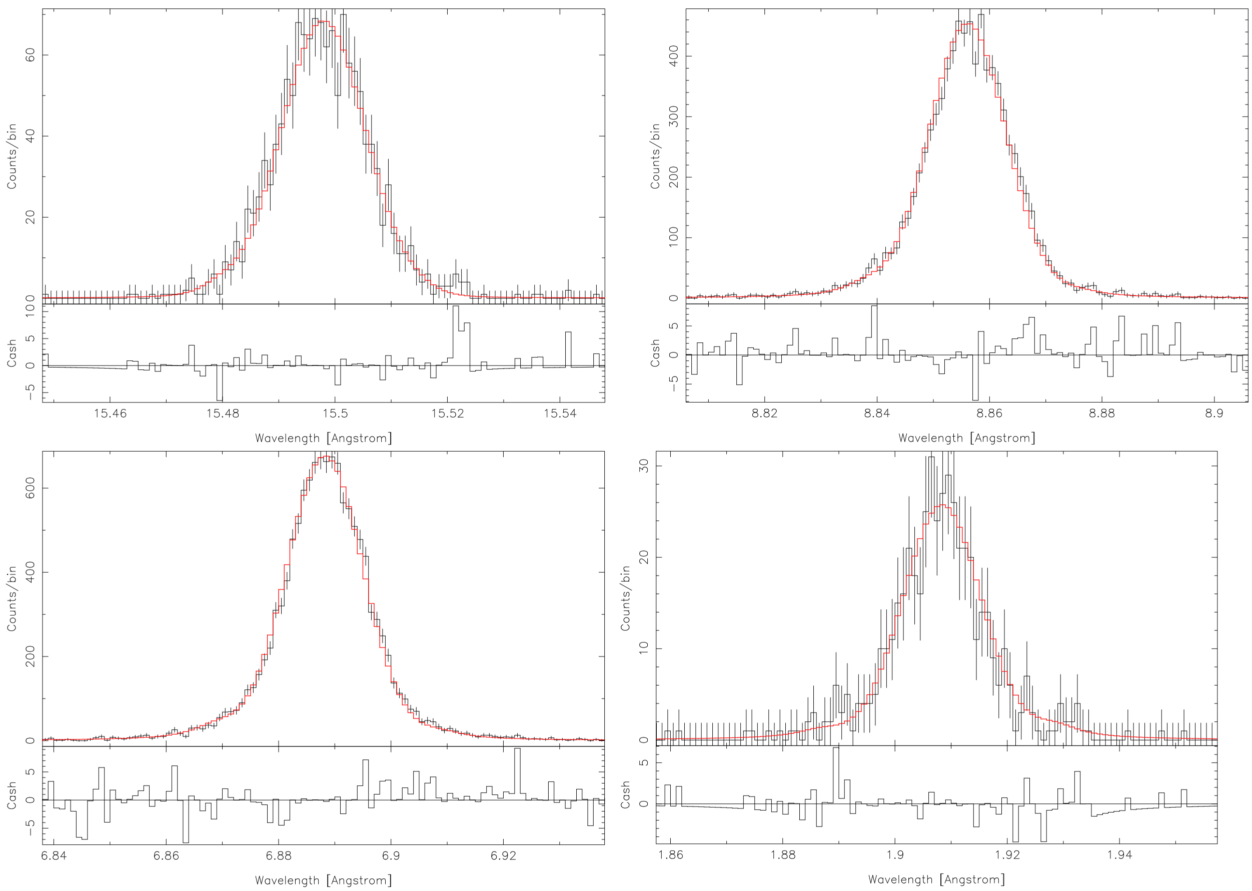

Figure 3: MEG +1st-order line profiles: (top left) line profile at E = 800 eV, with a goodness of fit $\chi^2 = 1.1$; (top right) E = 1400 eV, $\chi^2 = 1.5$; (bottom left) E = 1800 eV,χ^2 =1.6; and (bottom right) E = 6500 eV, $\chi^2 = 0.86$. In some cases the model fitting has resulted in goodness of fit slightly larger than unity.

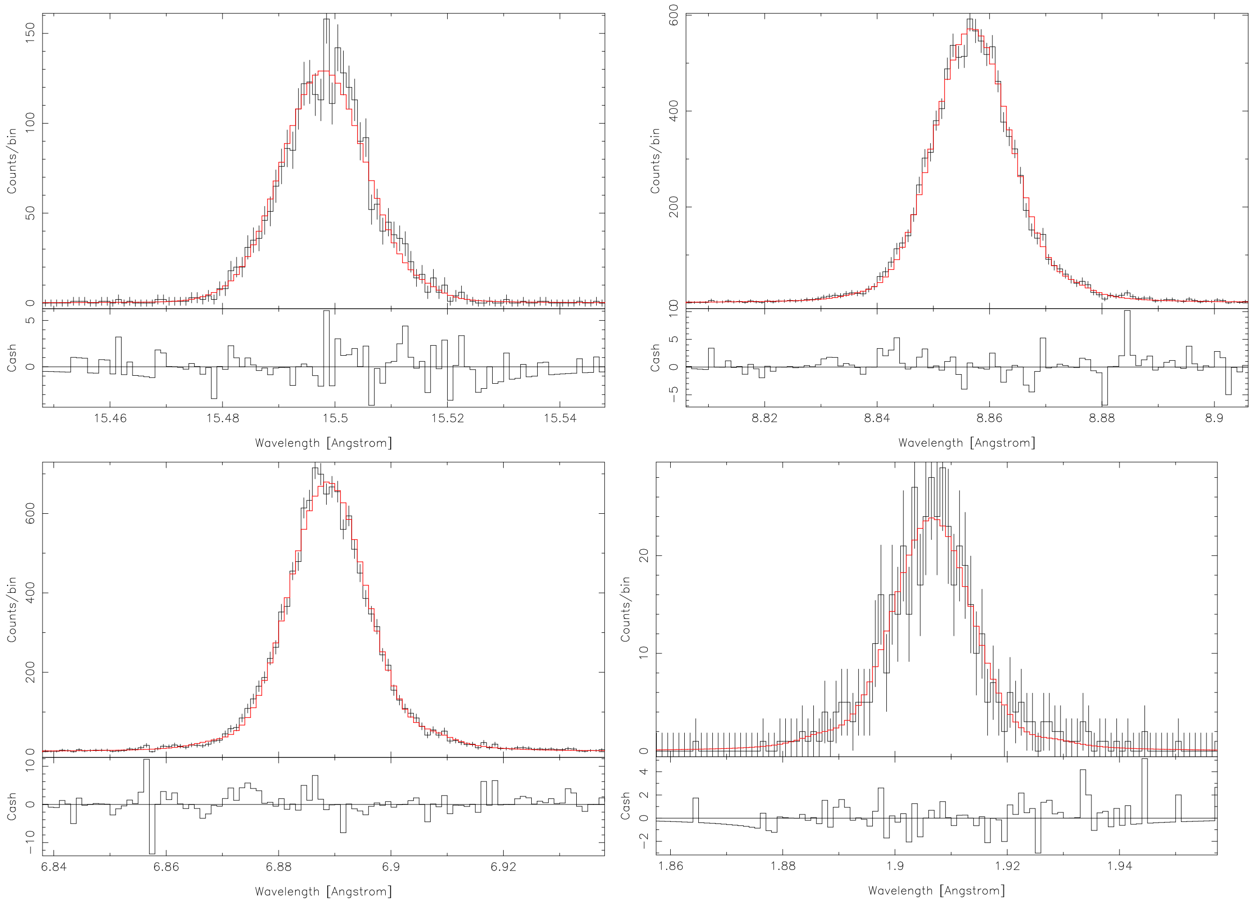

Figure 4: MEG -1st-order line profiles: (top left) line profile at E = 800 eV, with a goodness of fit χ^2 = 1.1; (top right) E = 1400 eV, χ^2 = 1.2; (bottom left) E = 1800 eV,χ^2 =1.7; and (bottom right) E = 6500 eV, χ^2 = 0.79. In some cases the model fitting has resulted in goodness of fit slightly larger than unity.

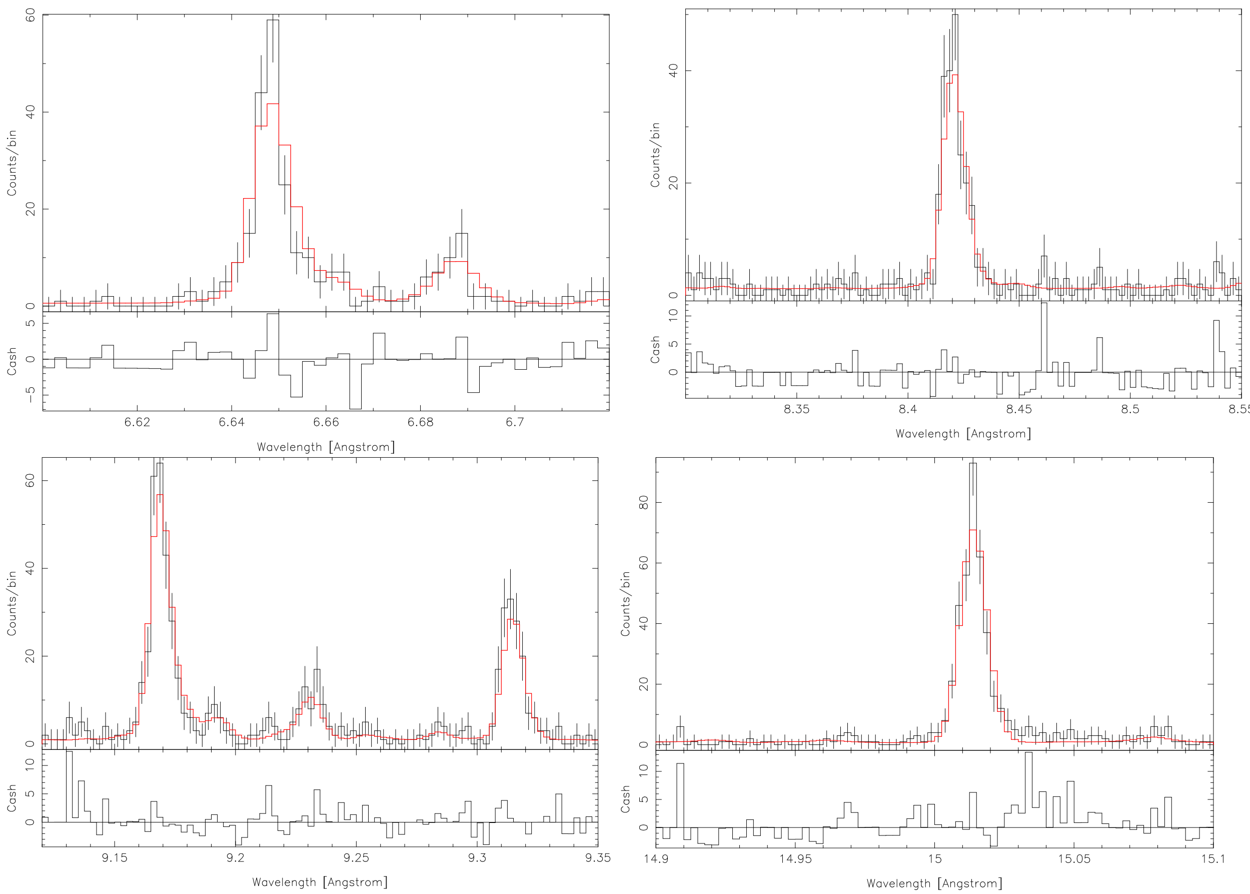

Figure 5: HEG +1st-order Capella line profiles; (top left) Si XIII He-like triplet lines, fitted with an APED thermal model (red) and its goodness of fit $\chi^2 = 1.69$; (top right) Mg XII H-like doublet line, with $\chi^2 = 1.69$; (bottom left) Mg XI He-like triplet lines, with $\chi^2 = 1.54$; and (bottom right) Fe XVII doublet line, with $\chi^2 = 2.04$. This simplified APED model (not necessarily the best fit) can adequately describe the Capella line spectra, though some neighboring lines are occasionally missing, which lead to higher χ^2 values.

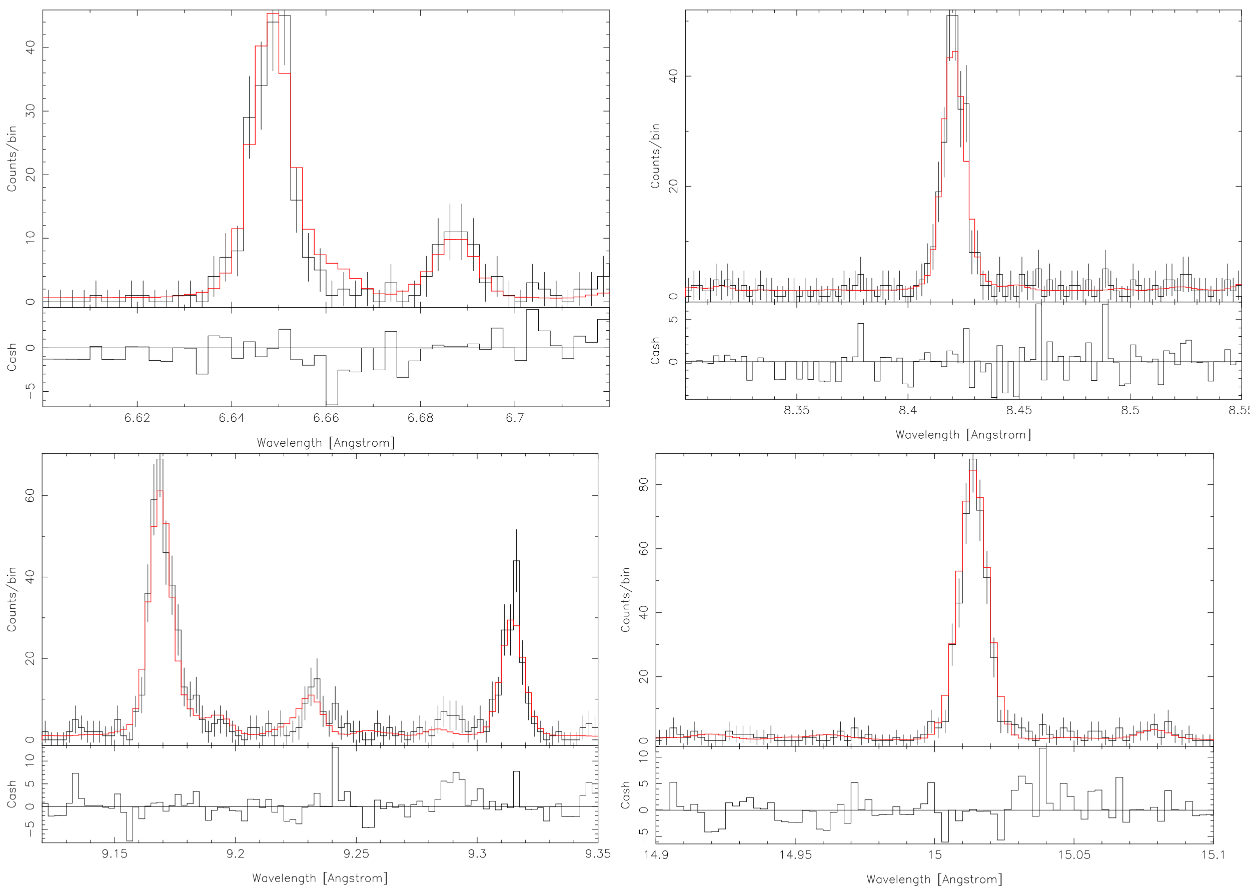

Figure 6: HEG -1st-order Capella line profiles; (top left) Si XIII He-like triplet lines, with goodness of fit $\chi^2 = 1.72$; (top right) Mg XII H-like doublet line, with $\chi^2 = 1.23$; (bottom left) Mg XI He-like triplet lines, with $\chi^2 = 2.02$; and (bottom right) Fe XVII doublet line, with $\chi^2 = 2.02$.

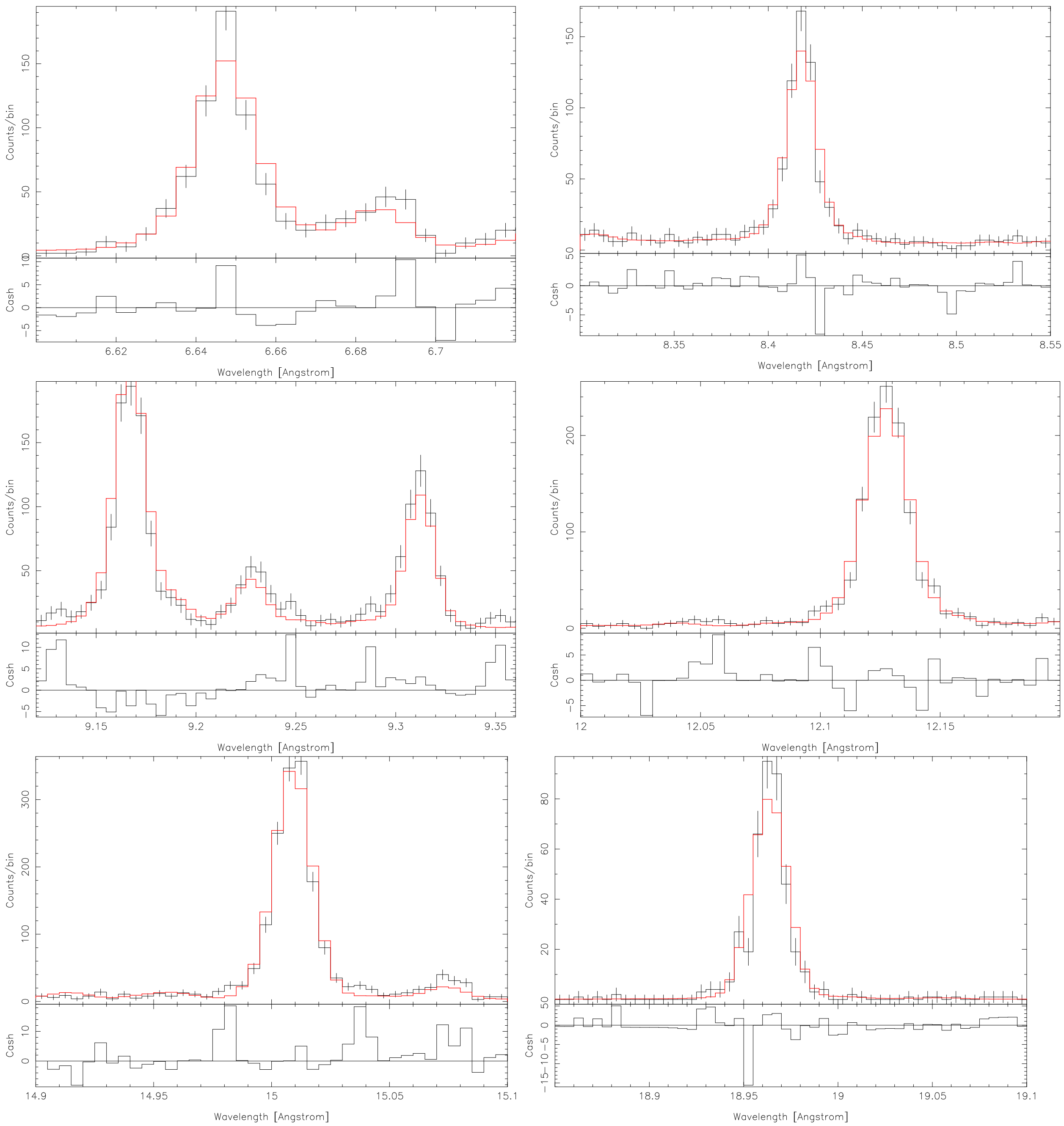

Figure 7: MEG +1st-order Capella line profiles; (top left) Si XIII He-like triplet lines, with goodness of fit $\chi^2 = 3.37$; (top right) Mg XII H-like doublet line, with $\chi^2 = 1.24$; (middle left) Mg XI He-like triplet lines, with $\chi^2 = 3.28$; (middle right) Ne X and Fe XVII blend, with with $\chi^2 = 2.23$; (bottom left) Fe XVII doublet line, with $\chi^2 = 4.48$; and (bottom right) O VIII line, with $\chi^2 = 1.86$. The high χ^2 values results from a poorly defined APED thermal model (i.e., missing neighboring lines).

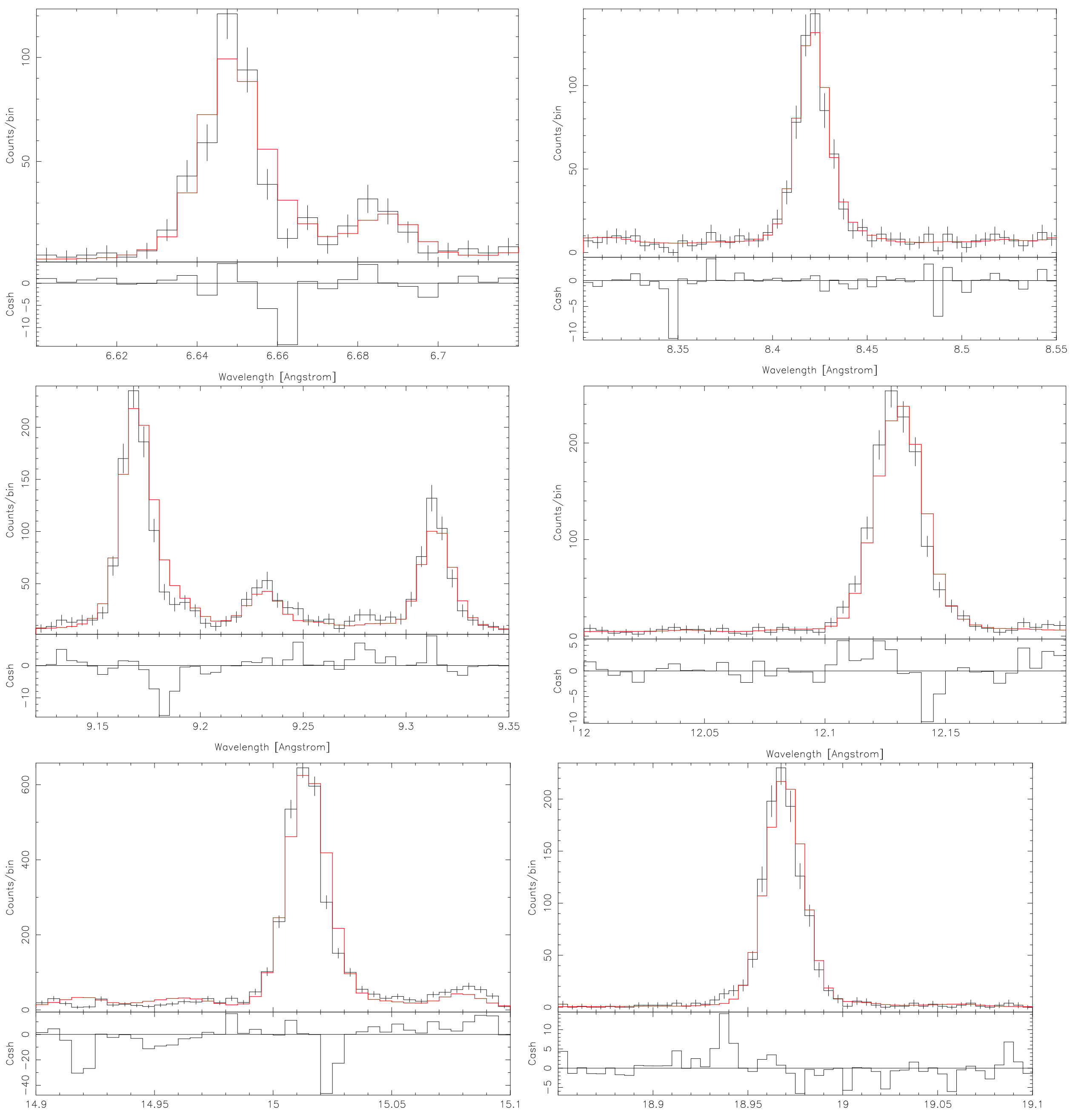

Figure 8: MEG -1st-order Capella line profiles; (top left) Si XIII He-like triplet lines, with goodness of fit $\chi^2 = 2.45$; (top right) Mg XII H-like doublet line, with $\chi^2 = 1.26$; (middle left) Mg XI He-like triplet lines, with $\chi^2 = 2.59$; (middle right) Ne X and Fe XVII blend, with with $\chi^2 = 2.23$; (bottom left) Fe XVII doublet line, with $\chi^2 = 8.64$; and (bottom right) O VIII line, with $\chi^2 = 2.38$. Again, the high χ^2 values results from a poorly defined APED thermal model.

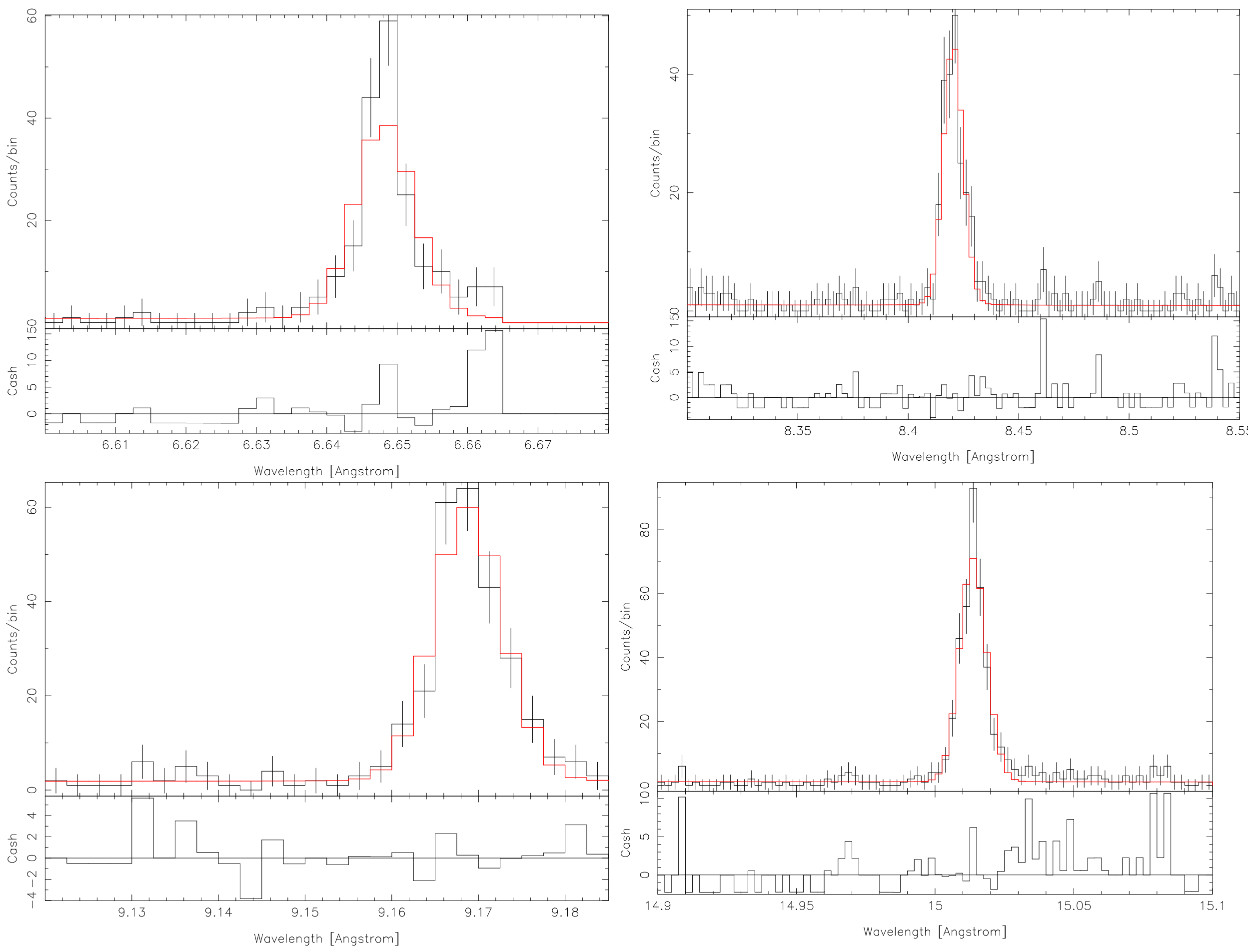

Figure 9: HEG +1st-order Capella line profiles; (top left) Si XIII He-like triplet lines, fitted with a single Gaussian function (red; velocity width $dv \approx 88$km s^{-1}) and its goodness of fit $\chi^2 = 2.94$; (top right) Mg XII H-like doublet line ($dv \approx 83$km s^{-1}), with $\chi^2 = 1.81$; (bottom left) Mg XI He-like triplet lines ($dv \approx 42$km s^{-1}), with $\chi^2 = 1.26$; and (bottom right) Fe XVII doublet line ($dv \approx 48$km s^{-1}), with $\chi^2 = 1.92$.

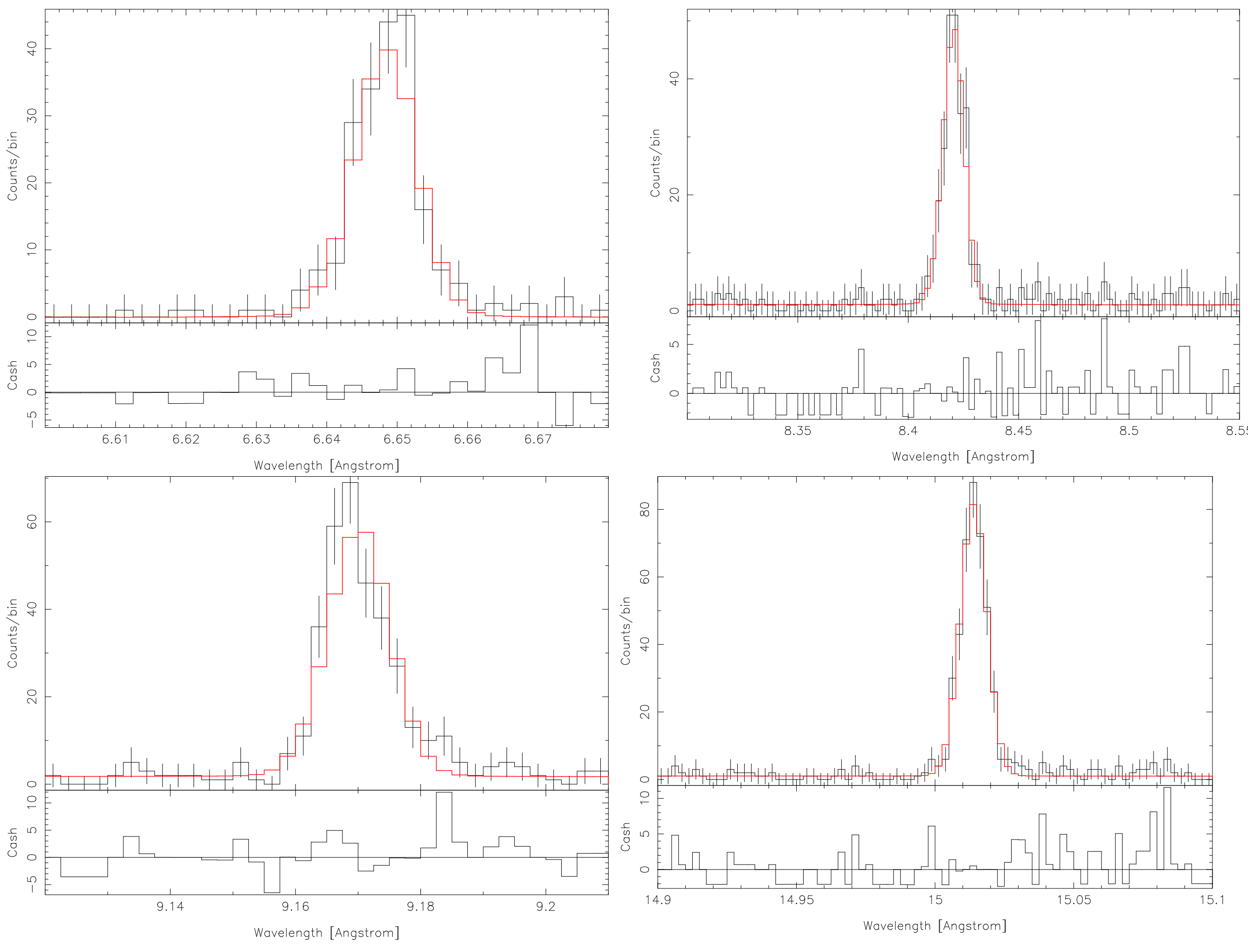

Figure 10: HEG -1st-order Capella line profiles; (top left) Si XIII He-like triplet lines, fitted with a single Gaussian function (red; velocity width $dv \approx 110$km s^{-1}) and its goodness of fit $\chi^2 = 0.68$; (top right) Mg XII H-like doublet line ($dv \approx 106$km s^{-1}), with $\chi^2 = 1.31$; (bottom left) Mg XI He-like triplet lines ($dv \approx 104$km s^{-1}), with $\chi^2 = 2.25$; and (bottom right) Fe XVII doublet line ($dv \approx 47$km s^{-1}), with $\chi^2 = 1.88$.

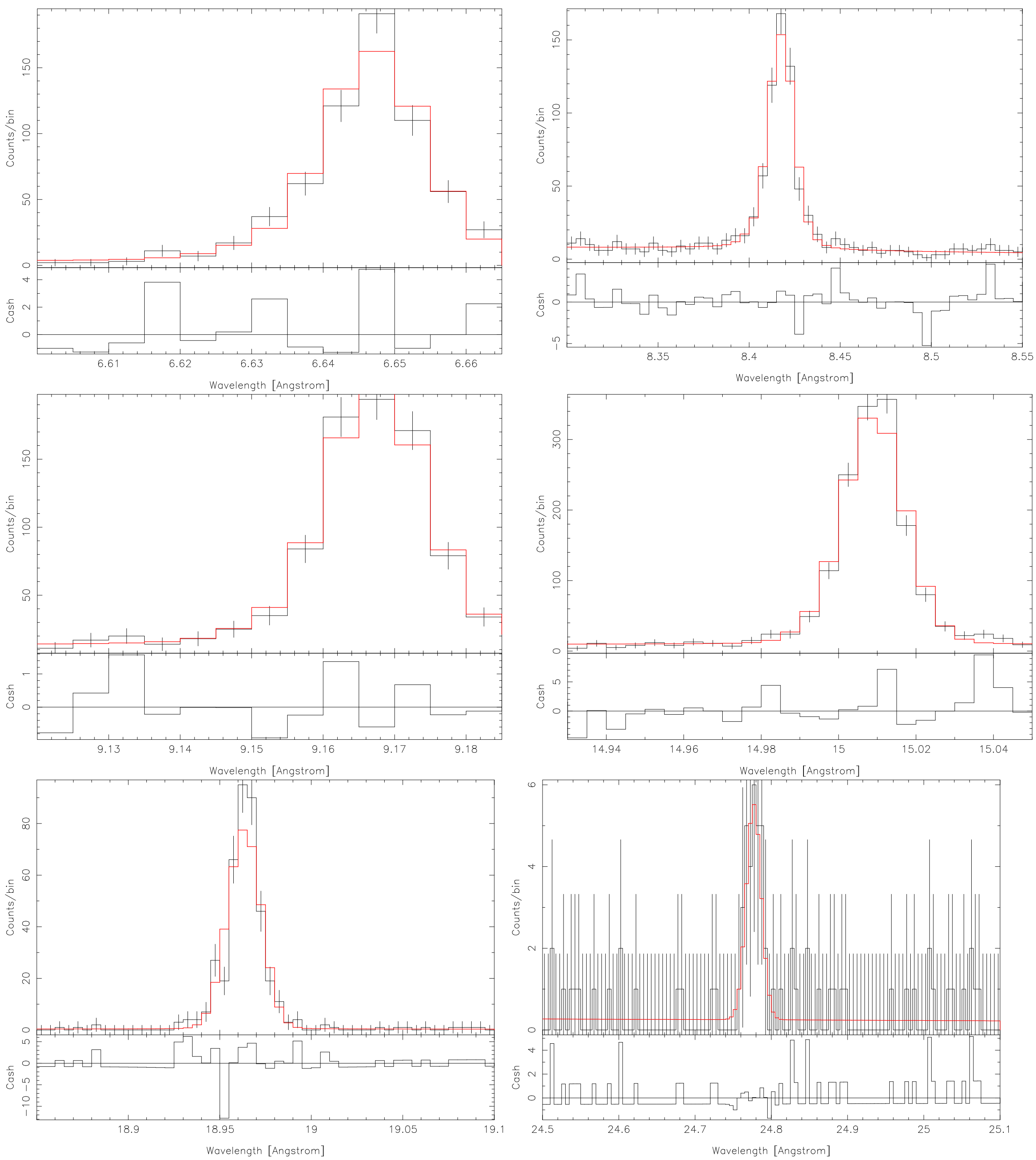

Figure 11: MEG +1st-order Capella line profiles; (top left) Si XIII He-like triplet lines, fitted with a single Gaussian function (red; velocity width $dv \approx 0$km s^{-1}) and its goodness of fit $\chi^2 = 2.26$; (top right) Mg XII H-like doublet line ($dv \approx 30$km s^{-1}), with $\chi^2 = 1.09$; (middle left) Mg XI He-like triplet lines ($dv \approx 19$km s^{-1}), with $\chi^2 = 0.97$; (middle right) Fe XVII doublet line ($dv \approx 29$km s^{-1}), with $\chi^2 = 2.29$; (bottom left) O VIII line ($dv \approx 48$km s^{-1}), with $\chi^2 = 1.67$; and (bottom right) N VII line ($dv \approx 36$km s^{-1}), with $\chi^2 = 0.93$.

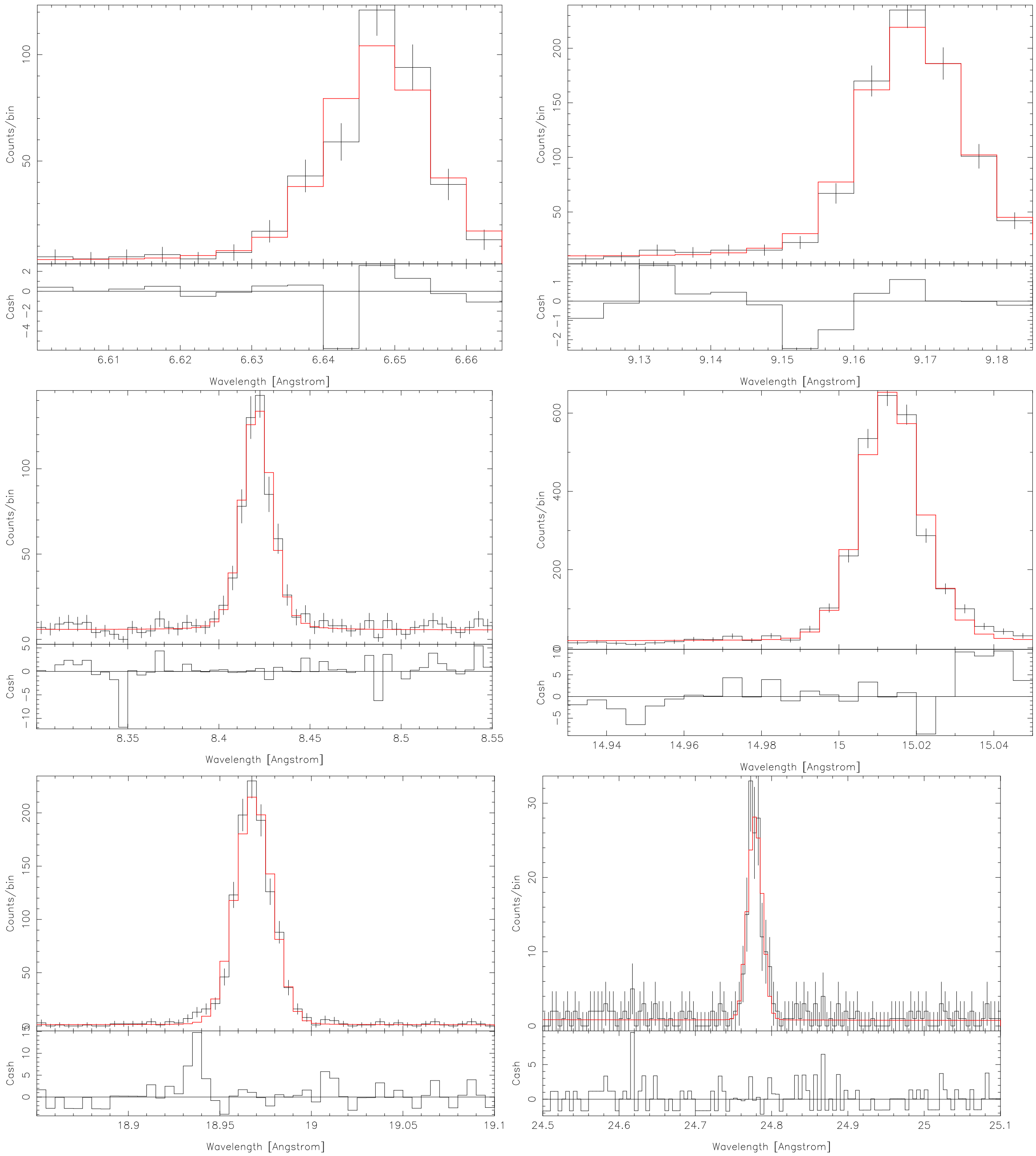

Figure 12: MEG -1st-order Capella line profiles; (top left) Si XIII He-like triplet lines, fitted with a single Gaussian function (red; velocity width $dv \approx 0.92$km s^{-1}) and its goodness of fit $\chi^2 = 1.40$; (top right) Mg XII H-like doublet line ($dv \approx 119$km s^{-1}), with $\chi^2 = 1.47$; (middle left) Mg XI He-like triplet lines ($dv \approx 25$km s^{-1}), with $\chi^2 = 1.07$; (middle right) Fe XVII doublet line ($dv \approx 20$km s^{-1}), with $\chi^2 = 3.75$; (bottom left) O VIII line ($dv \approx 78$km s^{-1}), with $\chi^2 = 2.06$; and (bottom right) N VII line ($dv \approx 0.11$km s^{-1}), with $\chi^2 = 1.35$.

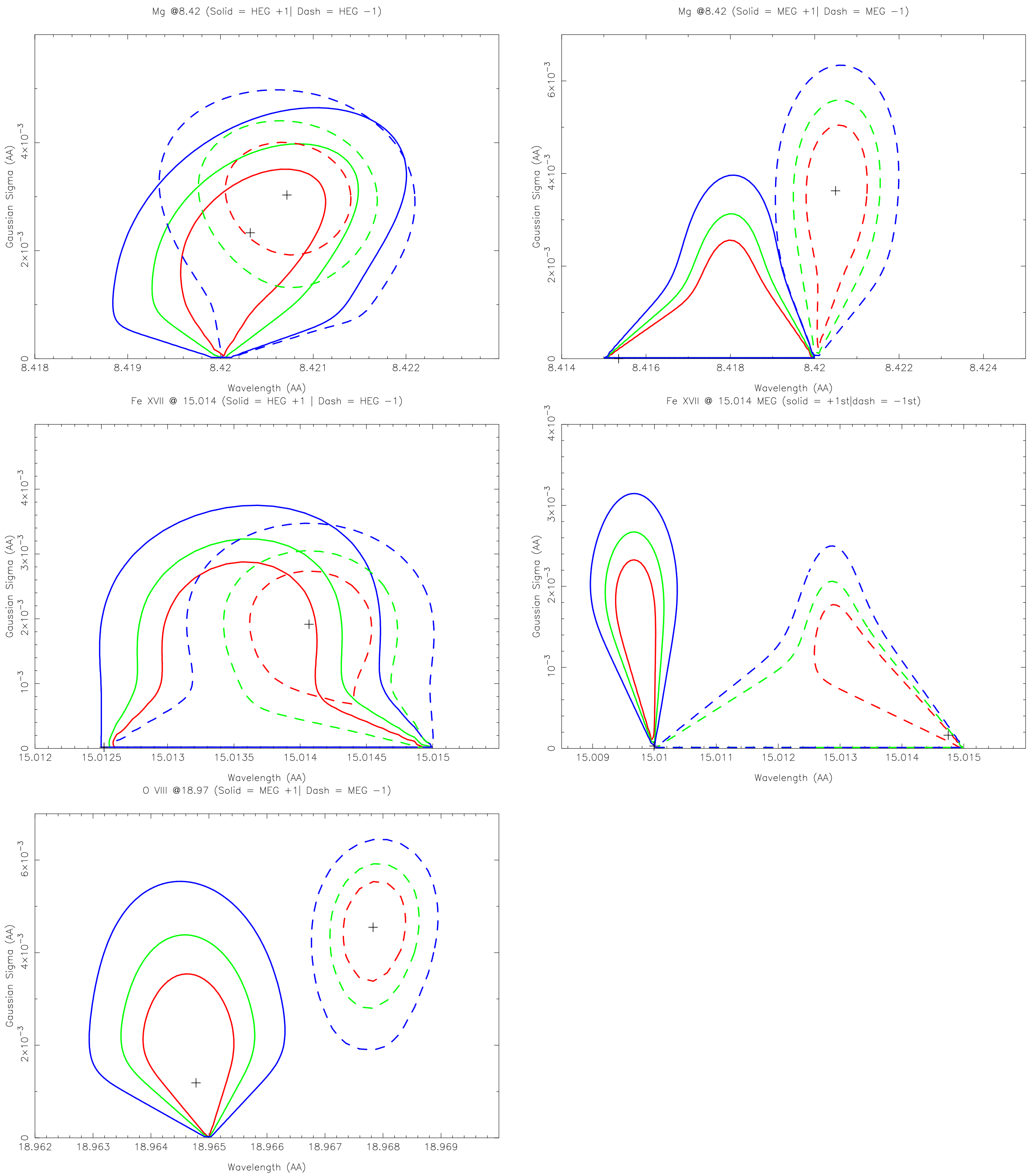

Figure 13: Confidence contour plots in Gaussian width vs. wavelength parameter space. Mg XI, Fe XVII, and O VIII lines (doublet lines) are selected for this exercise. The solid contour curves are for +1st order spectrum; and the dashed curves for -1st order. Note that, due to some calibration issues involved in MEG configuration, the ±1st contour levels do not overlap in the MEG datasets.

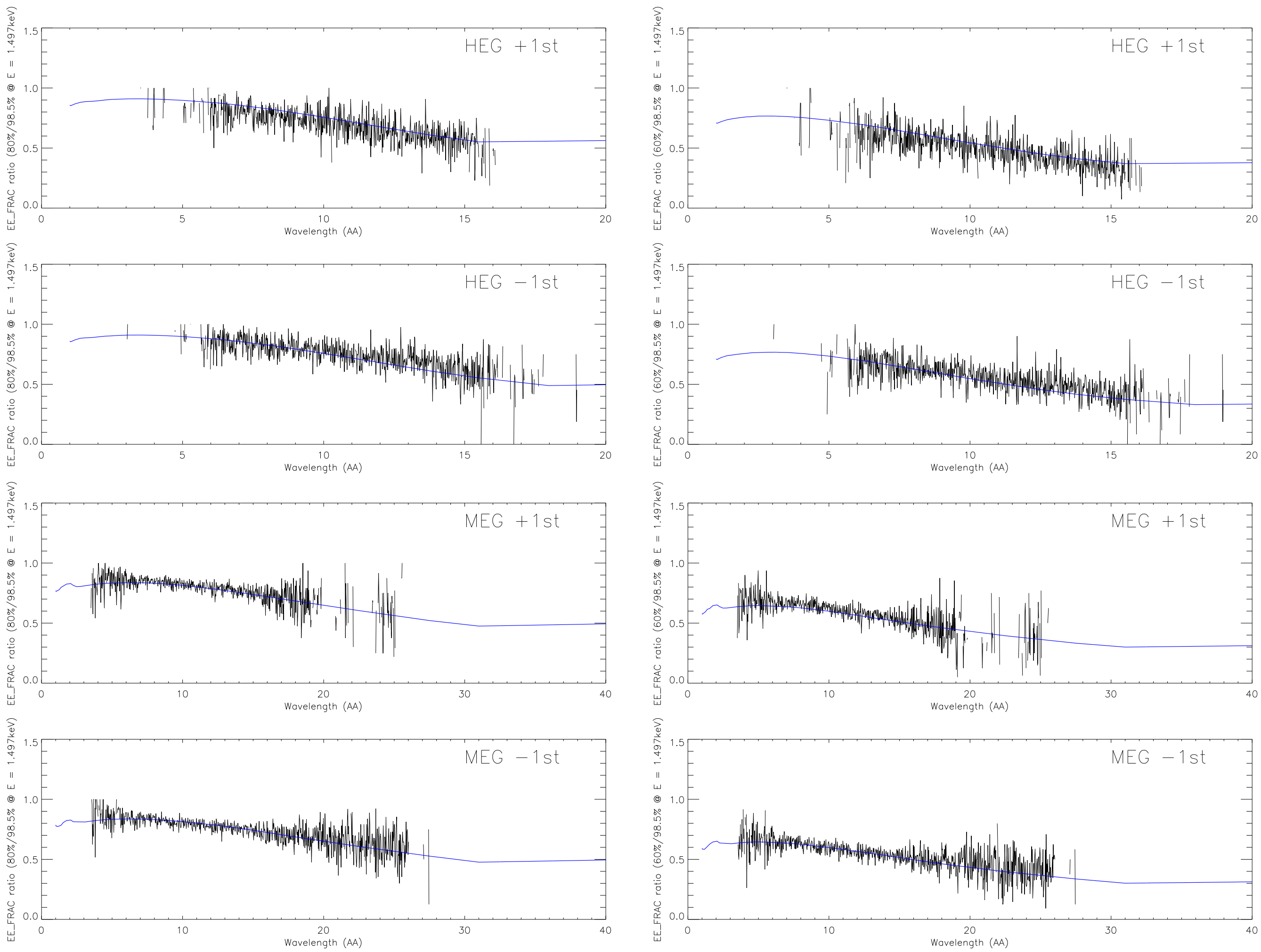

Figure 14: Ratio plots of theoretical (blue) and Capella's observed (black) EEFRAC values: (top 2 panels on left) HEG $\pm$1st, the ratio of Extraction B to A; (top 2 panels on right) HEG $\pm$1st, the ratio of Extraction C to A; (bottom 2 panels on left) MEG $\pm$1st, Extraction B to A; (bottom 2 panels on right) MEG $\pm$1st, Extraction C to A.

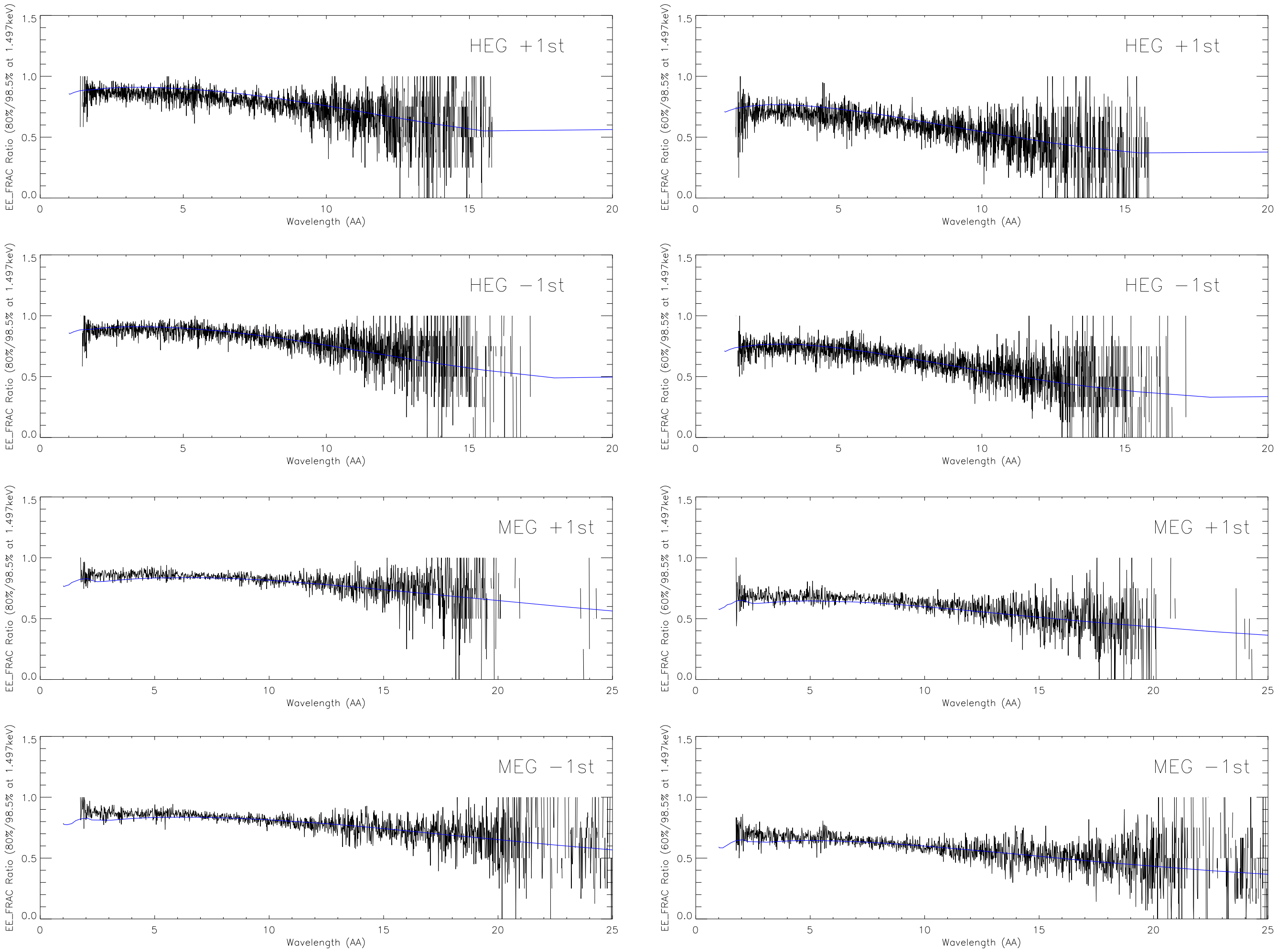

Figure 15: Ratio plots of theoretical (blue) and X1543-62's observed (black) EEFRAC values: (top 2 panels on left) HEG ±1st, the ratio of Extraction B to A; (top 2 panels on right) HEG ±1st, the ratio of Extraction C to A; (bottom 2 panels on left) MEG ±1st, Extraction B to A; (bottom 2 panels on right) MEG ±1st, Extraction C to A.